WARSAW UNIVERSITY OF TECHNOLOGY Index 351733
FACULTY OF CIVIL ENGINEERING
COMMITTEE FOR CIVIL AND WATER ENGINEERING
POLISH ACADEMY OF SCIENCES ISSN 1230-2945

DOI: 10.24425/ace.2022.143052

ARCHIVES OF CIVIL ENGINEERING

Vol. LXVIII ISSUE 4 2022

pp. 513–536

Research paper

Post buckling resistance reserve of corrugated girders with support stiffeners

Witold Basiński[1]

Abstract: The analysis of web-corrugated and trapezoidal profiled web girders focuses on the description of buckling resistance, possibly the ultimate resistance neglecting the post-buckling resistance reserve of girders. The problem is still the post-buckling resistance reserve and its possible application in practice. For this purpose this paper presents the analysis of tests on shear resistance of the corrugated web of SIN girders with the support stiffeners in the pre- and post-buckling zones. There are also presented values of the post-buckling resistance zone and the mutual relationships between pre- and post-buckling resistance zones. Values of these zones are related to optimization of the web-corrugated girders, which consists in enlarging the zone of pre-critical resistance and balancing between shear resistance and bending resistance. The experimental tests were performed on 20 girders with the following web depth: 500, 1000, 1250, and 1500 mm, composed of three pre-assembled units. The girders with a simply supported beam system and a simply supported beam with a single cantilever were made of pre-assembled units joined by means of high strength preloaded bolts. The numerical analysis by FEM was conducted for the models with web depth from h_w = 500 to 1500 mm at the full range of web thickness 2,0; 2,5, and 3 mm. The tests showed that stiffness of the support stiffeners in the web-corrugated girders had an impact on the size of pre- and post-buckling resistance zones, which consequently reduced the zone of post-buckling resistance. Because the initiated loss of stability of the corrugated-web girders is an irreversible and rapid process, and the resulting displacements in the non-linear area are permanent, the application of the post-buckling resistance zone in practice can be troublesome. From the standpoint of the structural reliability, however, the post-buckling zone provides a yield delay, i.e. it may be regarded as a safety margin. Therefore, its most possible reduction is required.

Keywords: finite element, girders with corrugated web type SIN, post-buckling zone, shear buckling resistance, support stiffener

[1]DSc., PhD., Eng., Silesian University of Technology, Faculty of Civil Engineering, ul. Akademicka 5, 43-300 Gliwice, Poland, e-mail: witold.basinski@polsl.pl, ORCID: 0000-0002-9306-4569

1. Introduction

Girders with corrugated web type SIN, which have recently become popular due to their favourable mass distribution, have webs of three basic nominal thickness values: 2.0, 2.5, and 3.0 mm, and a height from 333 to 1500 mm. Nowadays, there are also available additional nominal thickness values of the web: 4, 5, and 6 mm. Steel yield strength of corrugated webs f_y recommended by the manufacturer is 235 MPa or 355 MPa [1].

Since the sheet corrugation is made by web stiffeners, its stiffness and elastic buckling shear stress increase [2–7]. The buckling mechanism for corrugated web is classified separately as local or global buckling [1, 2]. But no description of the post-buckling resistance reserve is given. On the other hand, local buckling of the trapezoidal corrugated web is classified as the interactive one [8–14]. Shear buckling resistance for the girders with trapezoidal corrugated webs is estimated by calculating the interactive buckling resistance. In the common Moon solution [12] 2009 based on the interactive buckling resistance Yi [15] and slenderness λ_s, the buckling resistance was reduced to the value of yield strength at shearing τ_y.

$$\frac{\tau_{n,M}}{\tau_y} = \begin{cases} 1.0 & \text{for } \lambda_s \le 0.6 \\ 1 - 0.614\,(\lambda_s - 0.6) & \text{for } 0.6 < \lambda_s \le \sqrt{2} \\ 1/\lambda_s^2 & \text{for } \sqrt{2} < \lambda_s \end{cases} \tag{1.1}$$

Similarly in the solution suggested by Sause and Braxtan in 2011 [14], buckling resistance expressed by the equation (2) was depended on the interactive slenderness and was reduced to the yield strength at shearing τ_y.

$$\tau_{n,SB} = \tau_y \left(\frac{1}{\lambda_{I,3}^6 + 2} \right)^{1/3} \tag{1.2}$$

However, for the sinusoidal corrugated webs similarly as for to the trapezoidal corrugation, the solution related to the interactive critical buckling based on the regression analysis from the FEM tests was proposed by Eldib in 2009 [16]. The author allowed for exceeding the yield strength and did not limit the failure to the girder as the whole. Thus, there was no description of the zone of post-buckling resistance of the girders with both corrugated and trapezoidal webs.

On the other hand, the papers [17–19] demonstrated that the vertical stiffeners in the web-corrugated girders increased the shear buckling resistance of the corrugated web. In the computational model [18, 19], the shear buckling resistance based on calculating the interactive buckling resistance was limited to the yield strength at shearing. Hence, shear resistance of the girders was safely limited to the buckling load:

$$V_{Rd} = V_{bw,Rd} = \tau_{nS,R,BA} h_w t_w \tag{1.3}$$

using values of shear buckling resistance for stiffened and non-rigid end posts from the equations [19]:

$$\tau_{nS,BA} = \tau_y \left[\frac{2}{\lambda_{I,6}^6 + 5} \right]^{1/6} \tag{1.4}$$

$$\tau_{nR,BA} = \tau_y \left[\frac{2}{\lambda_{I,6}^6 + 7} \right]^{1/6} \tag{1.5}$$

where: $\lambda_{I,6}$ is the interactive slenderness depending on the tangent yield strength τ_y and shear interactive buckling resistance $\tau_{crI,6}$:

$$\lambda_{I,6} = \sqrt{\frac{\tau_y}{\tau_{crI,6}}} \tag{1.6}$$

The problem was still the post-buckling resistance reserve and its possible application in practice. For this purpose this paper presents the analysis of tests on shear resistance of the corrugated web of SIN girders with the support stiffeners in the pre- and post-buckling zones. There are also presented values of the post-buckling resistance zone and the mutual relationships between pre- and post-buckling resistance zones. These values were directly related to optimization of the web-corrugated girders, that is, reducing the pre-buckling resistance zone and balancing between shear and bending resistance. The experimental tests were performed on 20 girders with the following web depth: 500, 1000, 1250, and 1500 mm, composed of three pre-assembled units. The girders with a simply supported beam system and a simply supported beam with a single cantilever were made of pre-assembled units joined by means of high strength preloaded bolts. The numerical analysis by FEM was conducted for the models with web depth from $h_w = 500$ to $h_w = 1500$ mm at the full range of web thickness of 2.0; 2.5, and 3 mm.

2. Experimental investigations

The experimental tests were performed on three groups of the girders and were used to analyse shear buckling resistance of the corrugated web of SIN girders with support stiffeners in the pre- and post-buckling resistance zone. The girders with a simply supported beam system were classified into two first groups (Table 1), (Fig. 1a). The third group included 10 girders with a simply supported beam system with a cantilever (Table 1), (Fig. 1b).

All the girders with the corrugated web were designed and performed in accordance with the current literature and standards [1, 3].

All the pre-assembled elements of the tested girders were assembled with by means of M 20 ($h_w = 500$ mm) and M 24 bolts grade 10.9 ($h_w = 1000$ and 1500 mm) with resistance of the connection greater than that of the girders [3]. The girder webs were made

Table 1. Experimental girders parameters

Girder	Web $h_w \times t_w$ [mm]	Flange $b_f \times t_f$ [mm]	Support stiffener [mm]	Span L/w_s [mm]	Static scheme
I group					
M 1.11	500 × 2	300 × 15	25 × 300	7000	beam
M 1.21	1000×2.5	300 × 15	25 × 300	7825	beam
M 1.31	1000×2.5	300 × 20	25 × 300	7825	beam
M 1.41	1250 × 2	300 × 15	25 × 300	7825	beam
M 1.51	1500 × 2	300 × 15	25 × 300	7825	beam
M 2.11	500 × 2.5	300 × 15	25 × 300	5000	beam
II group					
M 2.21	1000 × 2	300 × 15	25 × 300 + tee bar	5825	beam
M 2.31	1000×2.5	300 × 15	25 × 300 + tee bar	5825	beam
M 2.41	1000 × 3	300 × 15	25 × 300 + tee bar	5825	beam
M 2.51	1500 × 3	300 × 15	25 × 300 + tee bar	5825	beam
III group					
M 1.12	500 × 2	300 × 15	2 × 20 × 300	5760/1000	beam+cantilever
M 1.22	1000 × 2	300 × 15	2 × 25 × 300	6000/1500	beam+cantilever
M 1.32	1000×2.5	300 × 20	2 × 25 × 300	6000/1500	beam+cantilever
M 1.42	1250 × 2	300 × 15	2 × 25 × 300	6000/1500	beam+cantilever
M 1.52	1500 × 2	300 × 15	2 × 25 × 300	6000/1500	beam+cantilever
M 2.12	500 × 2	300 × 15	2 × 20 × 300	4000/1000	beam+cantilever
M 2.22	1000 × 2	300 × 15	2 × 25 × 300	3750/1500	beam+cantilever
M 2.32	1000×2.5	300 × 15	2 × 25 × 300	3750/1500	beam+cantilever
M 2.42	1000 × 3	300 × 15	2 × 25 × 300	3750/1500	beam+cantilever
M 2.52	1500 × 2	300 × 15	2 × 25 × 300	3750/1500	beam+cantilever

of steel with the guaranteed yield strength $fy = 235$ MPa, and the flanges were made of steel S 275, as specified by the manufacturer.

The assembled girders were placed at the test stand. The frames (FR) were used to load the girders (Fig. 2). In case of the girders with a simply supported beam system, load exerted by a pair of forces $2P/2$ was transferred by means of the actuator (1) through the dynamometer (2) to the beam (3), and then to the tested girder (4) at the location of middle stiffeners. Movable (5) and fixed (6) bearings were put on the tested girder to support

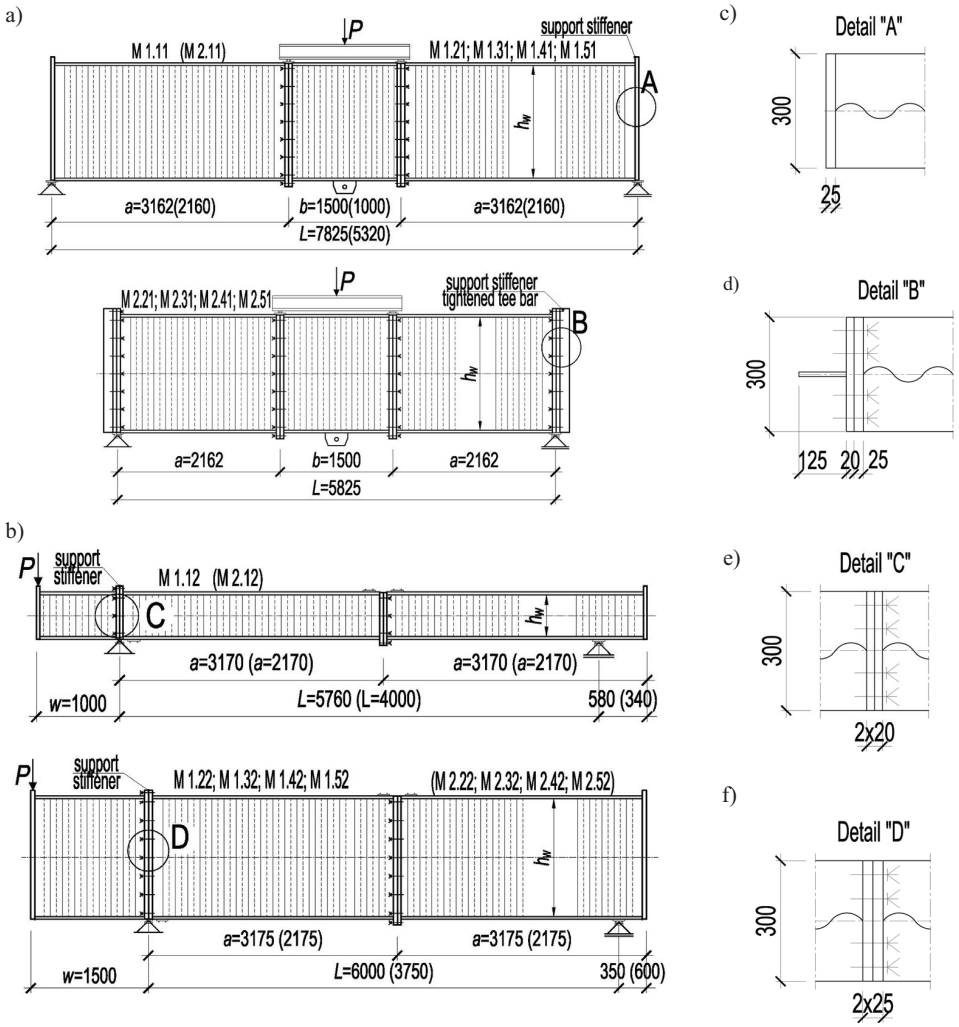

Fig. 1. Girders with corrugated web: a) beam girders b) cantilever girders; c) d) e) f) support stiffeners

the beam (3). Load in case of the girders with a simply supported beam system with the cantilever was transferred as the single concentrated force P by means of the actuator (1) through a washer (7) to the end plate of the cantilever part. Two dynamometers (2) for recording the reaction V versus load P were located below the support stiffener.

These tests were conducted to measure the load P acting on the beam girders, the reaction V in cantilever girders, the total deflection y of the girders with the transducers (8), and web strains with the gauges (9) to define the start of buckling. The load P of the girders was gradually increased by 2 kN until non-linear displacements of the girders. Then, the load increment was decreasing. The load was applied at the rate of 20 kN/min are reached.

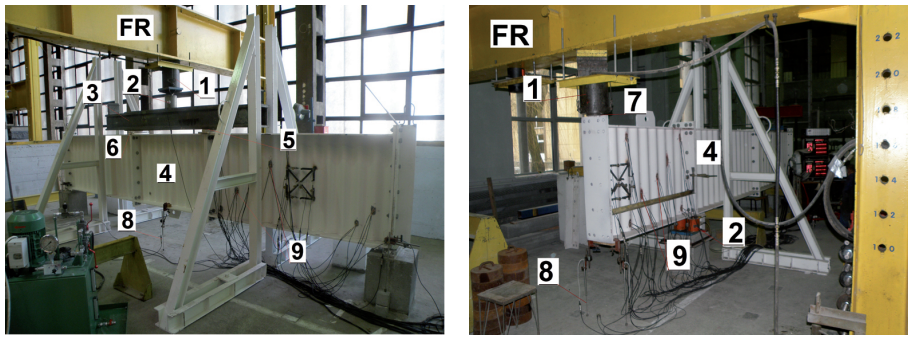

(a) (b)

Fig. 2. Example of girders on the test stand: a) girder 2.41; b) girder 2.42

3. Numerical tests

In case of the numerical analysis [20] of estimating shear buckling resistance of the corrugated web of SIN girders with support stiffeners within the post-buckling resistance zone, the tests were conducted on beam and cantilever girders (Table 2). Geometry of the girder numerical models was equivalent to that of the experimental girders. Because dimensions of the web, the support stiffeners, and the flanges affect the deformation shape in the web-corrugated girders, the geometry of the tested girders: their height, thickness and shape of web corrugation (during the material tests), of the end and intermediate stiffeners, and of the flanges was precisely measured. Straightness and curvature of the flanges were verified. The girders did not exhibit geometric imperfections both in longitudinal and

Table 2. Girder models parameters

h_w [mm]	t_w [mm]	Flange [mm]	Support Stiffener [mm]	w [mm]	a [mm]	b [mm]	L [mm]	Number of models
500–1500	2; 2.5; 3	300 × 15	300 × 25	–	3162	1500	7825	12
500–1500	2; 2.5; 3	300 × 15	300 × 25 + tee bar	–	3162	1500	7825	12
500–1500	2; 2.5; 3	300 × 15	300 × 25	–	2162	1500	7825	12
500–1500	2; 2.5; 3	300 × 15	300 × 25 + tee bar	–	2162	1500	7825	12
500	2; 2.5; 3	300 × 15	2×300×20	1500	–	–	6000	3
1000	2; 2.5; 3	300 × 15	2×300×25	1500	–	–	6000	3
1250	2; 2.5; 3	300 × 15	2×300×25	1500	–	–	6000	3
1500	2; 2.5; 3	300 × 15	2×300×25	1500	–	–	6000	3

cross sections. The girders were protected against lateral torsional buckling to eliminate this effect. It was very important because the lack of alignment in transmitting load to the girder could affect a change in the deformation of the corrugated web. The reduced dimensions of web by 1/10 of its thickness were regarded as the geometric imperfection [4].

The range of web thickness and span values was extended for the numerical analysis. The rigid end plate connections in the numerical girders were replaced with intermediate stiffeners whose thickness corresponded to the total thickness of end-plates, that is 50 or 40 mm (at $h_w = 500$ mm). The numerical analysis was conducted on 60 girders divided into three groups: beam girders with non-rigid end posts (12 with $a = 3.16$ and 12 with $a = 2.16$), beam girders with stiffeners reinforced with tee bars (12 with $a = 3.16$ and 12 with $a = 2.16$), and the cantilever girders. In case of the cantilever girders, the modelled cantilevers had a length $w = 1500$ mm, and the internal element with a span $L = 6000$ mm. The corrugated web was modelled in the CAD environment as a sinusoidal shell and the following thickness values were taken: 2, 2.5, and 3 mm. The flanges, the stiffeners, and the web were modelled from the S4R (a 4-node doubly curved shell with reduced integration had six degrees of freedom at each node, three translations and three rotations) and S3 shell elements, which contained from 36488 (the model $h_w = 500$ mm) to 96417 (the model $h_w = 1500$ mm $L = 7825$) finite elements [20].

3.1. Materials testing

Strength tests of the steel parameters used in the experimental girders were performed in accordance with the standard EN [21] on six random specimens taken along the web corrugation from the middle part of the web each girder and on three specimens taken from the flanges. The selected results from materials testing of a few representative girders are presented in Table 3.

Table 3. Material properties

Girder	$\overline{f}_y$ [MPa]	$\overline{f}_u$ [MPa]	Percentage total elongation at maximum force (F_m) [%]	Percentage total elongation at fracture [%]	$\overline{f}_y$ [MPa]	$\overline{f}_u$ [MPa]	Percentage total elongation at maximum force (F_m) [%]	Percentage total elongation at fracture [%]	E [GPa]
	web				flange				
M 1.21	275.9	416.0	15.4	20.7	303.4	485.5	22.6	29.4	213
M 1.31	260.4	403.0	16.1	20.8	298.9	435.7	24.8	32.2	205
M 2.51	289.3	376.8	18.4	23.1	290.3	432.0	25.0	30.7	203
M 1.42	267.2	360.9	13.4	19.9	302.8	440.4	22.9	30.8	199
M 1.52	299.1	380.5	16.8	23.3	312.5	445.6	24.1	30.0	200
M 2.52	281.0	375.5	17.2	24.6	306.7	449.3	21.9	28.6	213

The material tests of the girders were characterized by a significant variation of results for the yield strength of the webs between the individual girders [22]. To standardize the results, the material parameters for all 60 numerical girders were taken from the results from materials testing of the girder M 2.52. (Table 3). Parameters of the materials used in the numerical analysis were close to the yield strength of the girders M 1.42, M 1. 52, and the beam girders M 1.21, M 1. 31 and M 2.51. Hence, they could be directly compared with the results obtained from the numerical analysis.

3.2. Type of numerical analysis, load and boundary conditions

The boundary conditions for the numerical girders (Fig. 3) were the same as for the experimental girders (Fig. 1). One end of the numerical girders was placed on the hinge support, while the other end was on the roller support on the external end stiffeners, which reflected the support used in the real structures. In case of the cantilever girders, the span part was slightly elongated. However, it did not affect the buckling load. On the other hand, the experimental girders were on the roller support, that is, the bearings, and on the hinge support, on which the girder end was also placed.

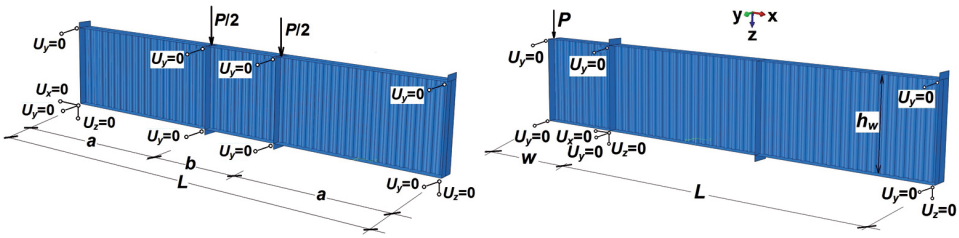

(a) (b)

Fig. 3. Boundary conditions of numerical girder: a) beams models b) cantilever models

For the hinge-sliding support, the vertical ($U_z = 0$), longitudinal ($U_x = 0$), and lateral ($U_y = 0$) displacements were blocked. For the edge support, the vertical ($U_z = 0$) and lateral ($U_y = 0$) displacements were blocked. To protect the girders from lateral torsional buckling (LTB), the vertical displacements ($U_y = 0$) at the stiffeners and the girder rotation around the axis $x(\phi_x = 0)$ were blocked.

Vertical load from the beam girders (Fig. 3a) as a pair of forces $2P/2$ was exerted on the intermediate stiffeners. For the cantilever girders, on the other hand, load (Fig. 3b) in the form of the concentrated force P was exerted on the stiffener at the end of the cantilever.

The Riks method was used in the numerical analysis to find the solution regardless of the type of the web buckling. It was related to the search of the static equilibrium in each step of iteration [23].

4. Analysis of buckling of corrugated web

4.1. Analysis of strains changes of experimental girders

To determine the point of beginning of the corrugated web buckling, courses of strains were analysed for diagonal strain gauges glued to the web. The strain gauges were arranged in the form of rosette in the direction of the greatest expected strains (Fig. 4). An angle between the strain gauges in the rosettes was 120°.

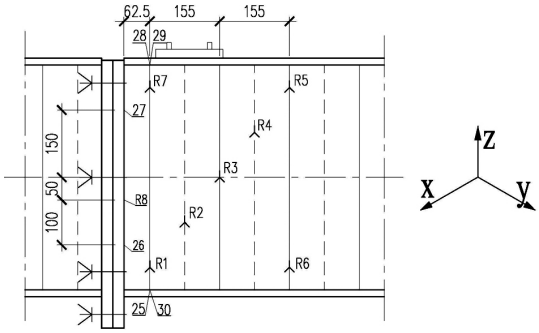

Fig. 4. Location of strain gauges on the girder web M 2.11

Based on the type of strains curves, the initial point of buckling of the corrugated web was determined and related to the buckling load P_{eB}. That load was specified for the point of losing the linear relationship between the load and strains $P(\varepsilon)$. The characteristic point $P_1(P_{eB})$ referred to buckling of the corrugated web, which was indicated by the initial change in the geometric shape of the wave under the buckling load P_{eB}. That point corresponded to the buckling resistance of the web. Buckling of the web in all the girders was observed at strain below 1/1000.

Fig. 5 illustrates the range of strains in the representative rosette R3 with strain gauges T1, T2, T3 (the girder M 1.32) which clearly indicates the strain changes in the main

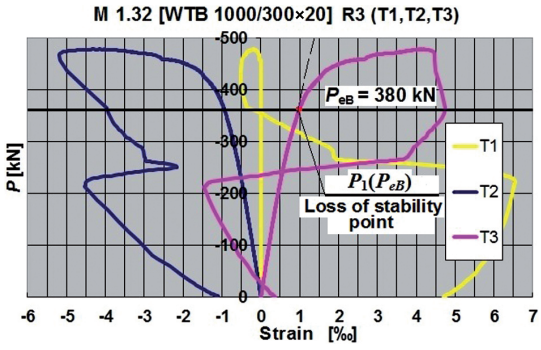

Fig. 5. Load-strains diagrams of the corrugated web in girder M 1.32 in a rosette R3

direction x (T3). Strains in the direction z recorded in the rosette R3 by the gauge T3 were minimal.

Fig. 6 illustrates examples of relationships between load and strain of individual rosettes in the main direction x of the tested girders with a simply supported beam with support stiffeners.

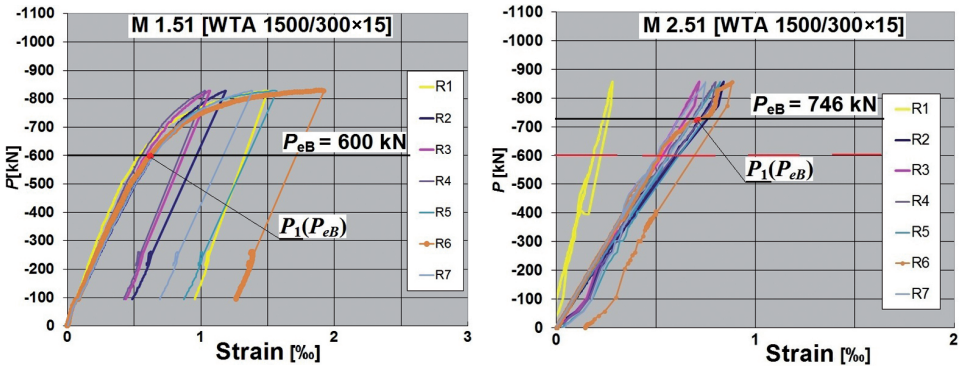

(a) (b)

Fig. 6. Load-strains diagrams of the corrugated web on main directions x: a) beam girders M 1.51 25 × 300 mm b) M 2.51 (25 × 300 mm + tee)

The linear range of strains in the graph $P(\varepsilon)$ was denoted as $0–P_1(P_{eB})$. The occurrence of local spots of buckling at the point $P_1(P_{eB})$ separated the linear part of strains from the non-linear ones. After exceeding the loading point $P_1(P_{eB})$, there was a notable increment in strains of the web due to bending and shearing. The influence of elastic-plastic displacements in the web caused by shear forces limited the flange resistance to the shear resistance of the corrugated web.

In the girders with the support stiffener reinforced by the tee bar, the range of elastic strains of the girder $0 – P_1(P_{eB})$ increased. That indicated an increase of the shear buckling resistance of the web. A dashed line in Fig. 6b illustrates how rigidity of the support stiffeners in the SIN girders increased by bolting the tee bars affected an increase in the linear range $0–P_1(P_{eB})$, that is, the buckling load against the girders with the end stiffener with a thickness of 25 mm. Increased stiffness of the support stiffeners was also correlated with an increased linear range of the web displacements. The comparison of both girders was justified despite the different length of the span a, because the impact of the span a at $a > h_w$ on the failure mode of the web, and on limit and buckling loads was regarded as negligible.

It should be noted that the load-strain $P(\varepsilon)$ relationship generally corresponded to the nature of the load-displacement paths $P(z)$. The buckling point for the girders was correlated with the course of the girder failure in accordance with the Subsection 4.3.

The experimentally-determined values of the buckling load P_{eB} and the boundary load P_{uR} of the girders with the support stiffeners at the free end and with a single cantilever are shown in Tables 4 and 5. The failure modes described in the Subsection 4.3 are denoted in

Table 4. Summary of test results for girders with support stiffener

Girder	Web $h_w \times t_w$ [mm]	Support stiffener	Failure modes	Lowest linear buckling load P_{eB} [kN]	Ultimate load $P_{u,R}$ [kN]	Buckling zone 0–$P_1(P_{eB})$	Post-buckling zone $P_1(P_{eB})$ – $P_2(P_{uR})$
1	2	3	4	5	6	7	8
M 1.11	500 × 2	20 × 300	L	260	330	0,79	0,21
M 2.11	500 × 2.5	20 × 300	L	280	436	0,64	0,36
M 1.21	1000×2.5	25 × 300	I	570	725	0,79	0,21
M 1.31	1000×2.5	25 × 300	I	605	745	0,81	0,19
M 1.41	1250 × 2	25 × 300	I	600	850	0,71	0,29
M 1.51	1500 × 2	25 × 300	I	600	828	0,72	0,28
M 2.21	1000 × 2	25 × 300 + tee	I	570	621	0,92	0,08
M 2.31	1000×2.5	25 × 300 + tee	I	740	894	0,83	0,17
M 2.41	1000 × 3	25 × 300 + tee	I	830	1035	0,80	0,20
M 2.51	1500 × 2	25 × 300 + tee	I	746	857	0,79	0,21

Table 5. Summary of test results for cantilever girders

Girder	Web $h_w \times t_w$ [mm]	Suport stiffener	Failure modes	Lowest linear buckling load P_{eB} [kN]	Ultimate load P_{uR} [kN]	Buckling zone 0–$P_1(P_{eB})$	Post-buckling zone $P_1(P_{eB})$ – $P_2(P_{uR})$
1	2	3	4	5	6	7	8
M 1.12	500 × 2	2×20×300	L	147	184	0,80	0,20
M 2.12	500 × 2	2×20×300	L	151	181	0,83	0,17
M 1.22	1000 × 2	2×25×300	I	298	342	0,87	0,13
M 2.22	1000 × 2	2×25×300	L	296	343	0,86	0,14
M 1.32	1000×2.5	2×25×300	I	380	478	0,79	0,21
M 2.32	1000×2.5	2×25×300	I	390	492	0,79	0,21
M 2.42	1000 × 3	2×25×300	I	510	694	0,73	0,27
M 1.42	1250 × 2	2×25×300	I	304	348	0,87	0,13
M 1.52	1500 × 2	2×25×300	I	400	468	0,85	0,15
M 2.52	1500 × 2	2×25×300	I	399	459	0,79	0,21

the tables in the following way: L – local mode of failure, I – interactive mode of failure. Relative values of pre- and post-buckling zone of the tested girders are shown in columns 7 and 8.

4.2. Buckling point for numerical girders

The buckling point was correlated with the curve $Px(z)$ representing the load step (Px – connected to the search of the static equilibrium in each step of iteration in the Riks method) and was placed at the beginning of the iterative densification. The resulting curving of the diagram indicated the beginning of a change in the geometric shape of the web. The buckling process for the corrugated web in the numerical girders started at the stability failure point. Fig. 7 present the reference paths $P_x(z)$ with the determined beginning of the web buckling in the numerical girders 1250×2.5 with the stiffeners reinforced with the tee bar and 1250×2.5 with a single cantilever.

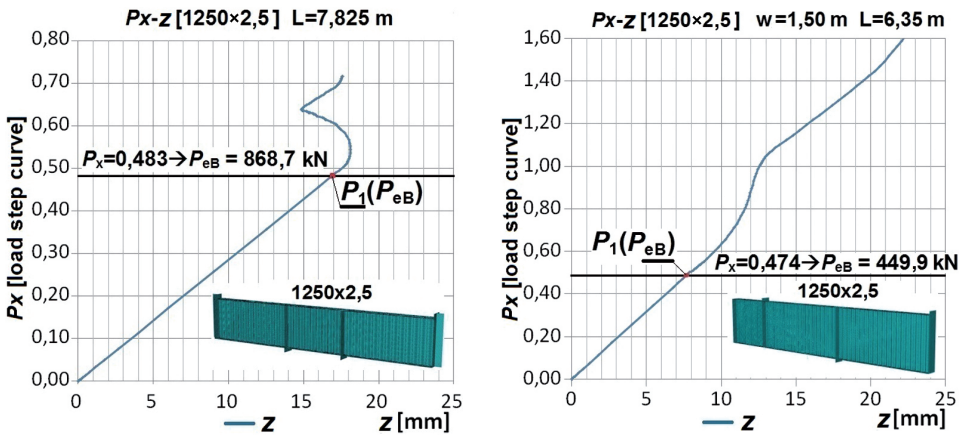

(a) (b)

Fig. 7. Load step curve vs displacement of example of numerical girders: a) with stiffener strengthen by tee 1250×2.5, b) with one-sided cantilever 1250×2.5

Tables 6 and 7 present the buckling load P_{eB} and the boundary load P_{uR} obtained from the numerical analysis for the numerical girders with the support stiffeners at the free and (for the support panel $a = 3$) and with a single cantilever, respectively. The failure modes described in the Subsection 4.3 are denoted in the tables in the following way: L – local mode of failure, I – interactive mode of failure. Values of pre- and post-buckling zone of the tested girders are shown in columns 6 and 7.

Table 6. Summary of the results of numerical analysis of numerical girders with support stiffeners

Web section $h_w \times t_w$ [mm]	Suport stiffener [mm]	Failure modes	Lowest linear buckling load P_{eB} $a = 3$ [kN]	Ultimate load P_{uR} $a = 3$ [kN]	Relative Pre-Buckling zone $0-P_1(P_{eB})$	Relative Post-buckling zone $P_1(P_{eB}) - P_2(P_{uR})$
1	2	3	4	5	6	7
500 × 2	20 × 300	L	262,1	288,8	0,91	0,09
500 × 2.5	20 × 300	L	330,3	361,7	0,91	0,09
500 × 3	25 × 300	L	395,1	434,4	0,91	0,09
1000 × 2	25 × 300	I	527,1	577,9	0,91	0,09
1000×2.5	25 × 300	I	659,7	724,5	0,91	0,09
1000 × 3	25 × 300	I	791,3	870,2	0,91	0,09
1250 × 2	25 × 300	I	659,9	722,8	0,91	0,09
1250×2.5	25 × 300	I	823,7	904,8	0,91	0,09
1250 × 3	25 × 300	I	988,3	1086,7	0,91	0,09
1500 × 2	25 × 300	I	796,2	867,9	0,92	0,08
1500×2.5	25 × 300	I	989,6	1085,9	0,91	0,09
1500 × 3	25 × 300	I	1185,5	1303,9	0,91	0,09
500 × 2	25 × 300 + tee	L	261,9	288,9	0,91	0,09
500 × 2.5	25 × 300 + tee	L	341,7	361,7	0,94	0,06
500 × 3	25 × 300 + tee	L	409,0	434,6	0,94	0,06
1000 × 2	25 × 300 + tee	I	556,5	578,0	0,96	0,04
1000×2.5	25 × 300 + tee	I	695,5	724,7	0,96	0,04
1000 × 3	25 × 300 + tee	I	843,5	870,6	0,97	0,03
1250 × 25	25 × 300 + tee	I	695,7	724,1	0,96	0,04
1250×2.5	25 × 300 + tee	I	868,7	906,2	0,96	0,04
1250 × 3	25 × 300 + tee	I	1041,9	1088,2	0,96	0,04
1500 × 2	25 × 300 + tee	I	839,5	869,4	0,97	0,03
1500×2.5	25 × 300 + tee	I	1042,9	1087,6	0,96	0,04
1500 × 3	25 × 300 + tee	I	1216,7	1305,8	0,93	0,07

Table 7. Summary of the results of numerical analysis of numerical cantilever girders

Web section $h_w \times t_w$ [mm]	Support stiffener [mm]	Failure modes	Lowest linear buckling load P_{eB} [kN]	Ultimate load P_{uR} [kN]	Relative pre-puckling zone $0-P_1(P_{eB})$	Relative post-buckling zone $P_1(P_{eB}) - P_2(P_{uR})$
1	2	3	4	5	6	7
500×2	$2 \times 20 \times 300$	L	149,1	154,1	0,97	0,03
500×2.5	$2 \times 20 \times 300$	L	186,8	192,2	0,97	0,03
500×3	$2 \times 20 \times 300$	L	224,6	231,3	0,97	0,03
1000×2	$2 \times 25 \times 300$	L	297,2	308,1	0,96	0,04
1000×2.5	$2 \times 25 \times 300$	I	371,3	384,3	0,97	0,03
1000×3	$2 \times 25 \times 300$	I	445,3	462,2	0,96	0,04
1250×2	$2 \times 25 \times 300$	I	360,1	384,6	0,94	0,06
1250×2.5	$2 \times 25 \times 300$	I	449,9	480,4	0,94	0,06
1250×3	$2 \times 25 \times 300$	I	539,5	576,5	0,94	0,06
1500×2	$2 \times 25 \times 300$	I	419,2	460,8	0,91	0,09
1500×2.5	$2 \times 25 \times 300$	I	531,9	575,6	0,92	0,08
1500×3	$2 \times 25 \times 300$	I	635,7	687,5	0,92	0,08

4.3. Failure modes of the girders with support stiffeners – the analysis of the buckling process

During the analysis of the buckling process for the corrugated web, failure of the low girders $h_w = 500$ mm and high ones $h_w = 1000$ mm should be distinguished by assigning buckling points which delimit the pre- and post-buckling zones.

For the low girders with a web depth of 500 mm with the support stiffeners, the buckling process began by local buckling of the sinusoidal panel in the straight section between the web corrugations. The point of buckling failure (PIUS-L) referred to the occurrence of the first local buckling point. After development of the local point of buckling, the yield line (2) was formed, beyond which the girder flanges were immediately loaded with shear force which led to flange bending in the girder plane (3) (Fig. 8).

However, for the girders with a web depth $h_w = 1000$ mm, buckling of the web separating the pre-buckling area from the post-buckling area began, as in case of lower girders, from local buckling between the tension flange and the girder axis. A few spots representing local buckling points of the web occurred in the initial phase. The points of buckling failure (PIUS-L) referred to a few local modes of buckling. In the next phase the local points evolved into global buckling, which resulted in the snap-through of adjacent

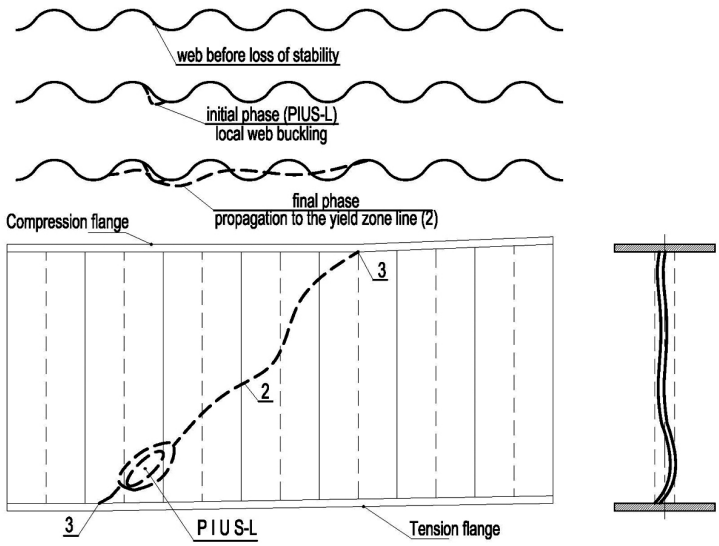

Fig. 8. Scheme of local instability of the sine wave girders with support stiffeners

groups of the web corrugations (1) in the opposite direction and was associated with the formation of yield zone lines (2) (Fig. 9). After the snap-through of the corrugations and the formation of the yield line, the girder flanges were immediately loaded with shear force which led to their bending in the girder plane (3). Local buckling points after their transformation into the snap-through of the web corrugations were connected and formed the buckling spectrum. In that case the local buckling of the web walls initiated the global mode of buckling. Thus, the local instability initiated the mechanism of the web failure leading to the global buckling of the web. It means the local instability had an impact on the global buckling, that is, there was an interaction between both failure modes.

The web failure in the described tests on the girders with the support stiffeners at the free end was observed in the area loaded with the constant shear force. In each tested girder with the scheme of a simply supported beam, the intermediate stiffener formed by the end plate connection was unaffected. The process of the corrugated web instability began from the local instability of the sinusoidal panel. After the occurrence of the local point of the web instability (PIUS-L) in the girders $h_w = 500$ mm (Fig. 10a), the yield line was formed at the tension flange (2) (Fig. 10b).

The process of losing stability of the corrugated web in the girders with a web depth from $h_w = 1000$ mm began from the occurrence of a few local buckling points presented as the initiation points of instability (Fig. 11a). Then, the process evolved to attain the global mode. That resulted in the snap-through of adjacent groups of the web corrugations (1) associated with the yield line (2) forming the so called buckling spectrum (the interactive instability – I) (Fig. 11b).

Regardless of the height and stiffness of the support stiffener, the local bulging of the web was observed in the numerical girders in the first phase of failure. The bulges represented

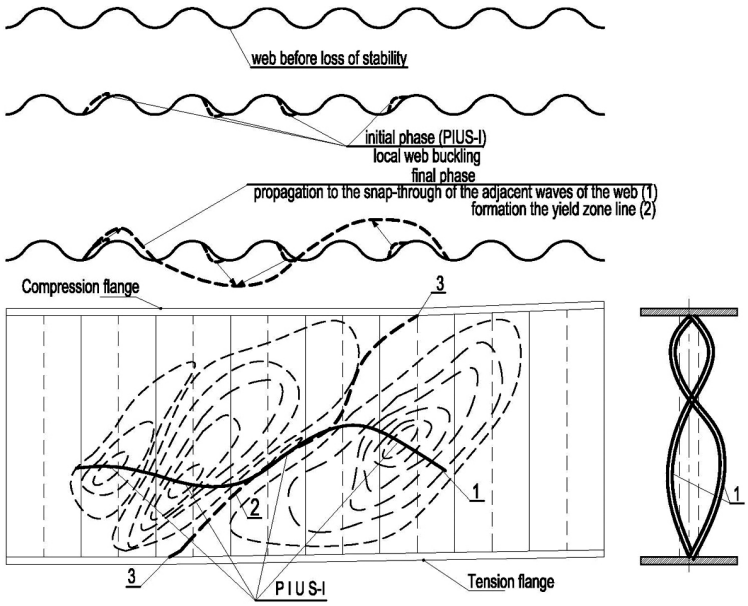

Fig. 9. Scheme of interactive instability (the transition from local to global phase) of the corrugated web of girders with support stiffeners (designations – description in the text)

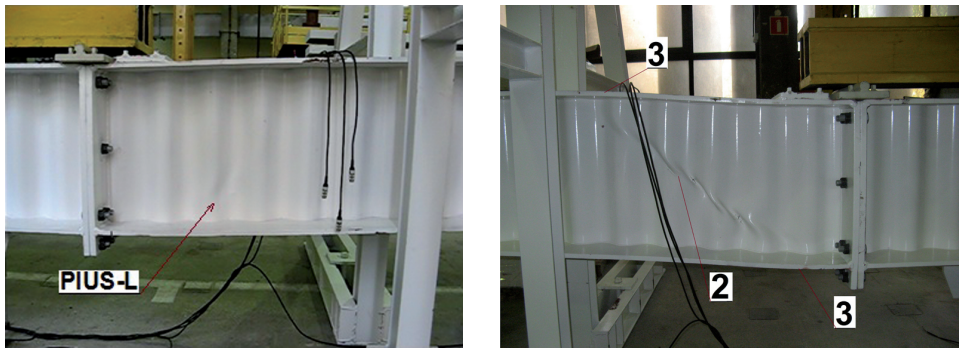

(a) (b)

Fig. 10. Stages of failure mode of girder with corrugated web M 2.11 (500 × 2.5): a) initiation point of instability (PIUS-L) of the girder web, b) final failure mode of the girder

the initiation point of instability of the numerical girders with a height $h_w = 500$ mm (PIUS-L in Fig. 12).

In the numerical girders with a low web having a height $h_w = 500$ mm, with the non-rigid and stiffened end posts, and in the cantilever girders, the yield line (2) was formed near the tension flange after local buckling of the web. It caused the immediate loading

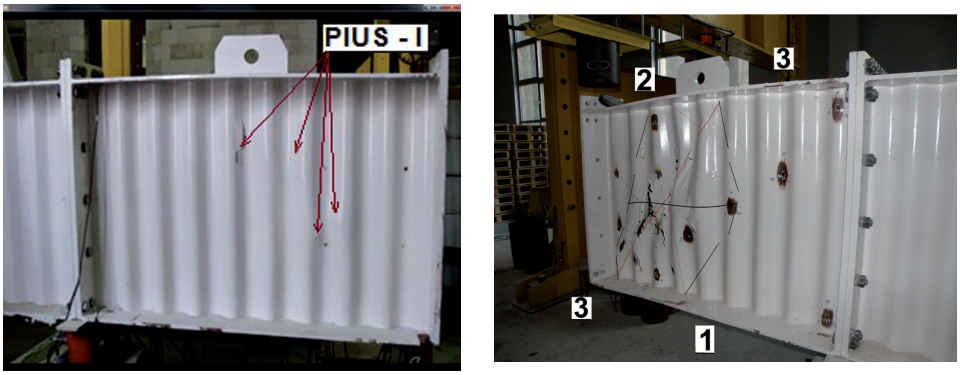

(a) (b)

Fig. 11. Stages of failure mode of SIN girders with cantilever: a) initiation points for the instability of the (PIUS-I) girder web M 2.32 (1000 × 2.5), b), final failure mode of the girders M 2.32 (1000 × 2.5)

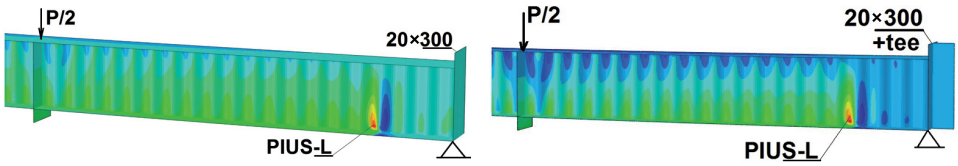

(a) (b)

Fig. 12. Initiation points of instability PIUS-L of numerical girders a) 500 × 2, b) 500 × 2 with tee

of flanges in the low girders h_w = 500 mm with the shear force, which caused the flange yielding in the plane of the girders. The failure modes obtained for the numerical girders with a web depth h_w = 500 mm corresponded to the failure modes of the experimental girders (Fig. 13).

After increasing the height of the numerical girders with the support stiffeners to h_w = 1000 mm, the failure mode of the web changed. In the first phase after reaching the buckling load, local buckling of the web (PIUS-I) appeared (Fig. 14). However, the local buckling of the web evolved in the next phase to the global mode with the snap-through of adjacent corrugations of the web (1) in the opposite direction and was associated with the formation of the yield line (2) (interactive instability – I). Immediately after the formation of the yield line, the girder flanges were loaded with the shear force which led to flange bending in the girder plane, and thus to the failure of the web frame.

The failure modes obtained for the numerical girders with a web depth from h_w = 1000 mm to h_w = 1500 mm with the support stiffeners corresponded to the failure modes of the experimental girders (Fig. 15). The impact of the flange length a at $a > h_w$ on the failure mode of the web, and on boundary and buckling loads was regarded as negligible.

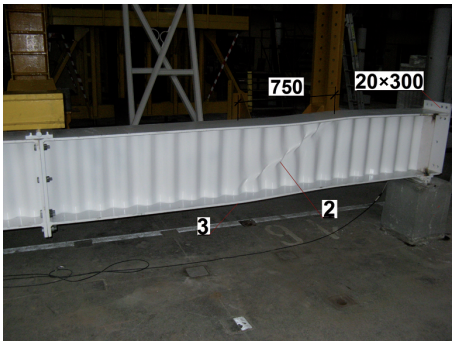

(a)

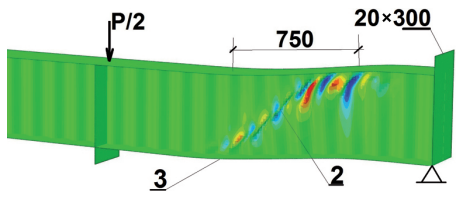

(b)

Fig. 13. Comparison of the failure modes: a) experimental girder M 1.11 (500 × 2), b) numerical girder 500 × 2

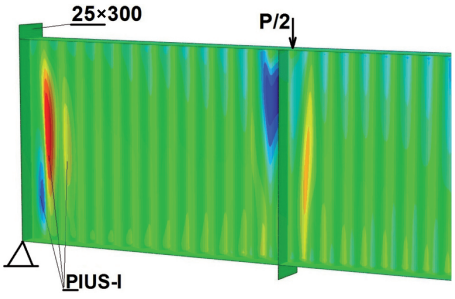

(a)

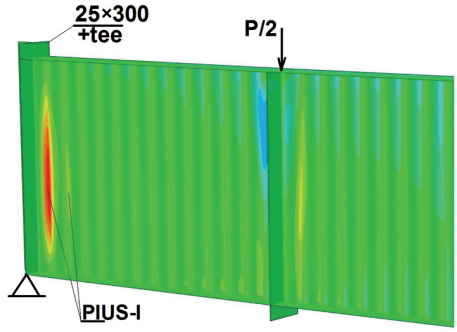

(b)

Fig. 14. Initiation points of instability PIUS-I of numerical girders a) 1500×2.5 b) 1500×2.5 with tee

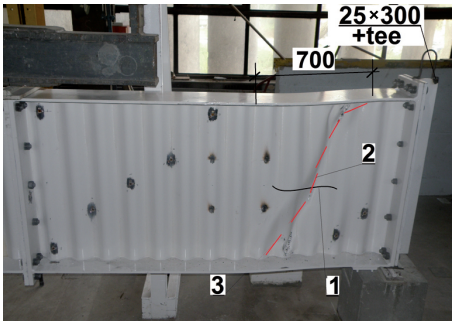

(a)

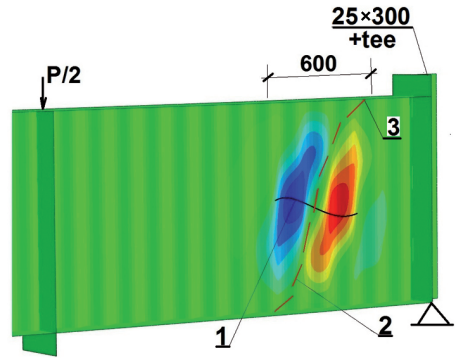

(b)

Fig. 15. Comparison of the failure modes: a) experimental girder M 2.31 (1000 × 2.5 + tee), b) numerical girder 1000 × 2.5 + tee

5. Influence of the support stiffeners stiffness on the post-buckling resistance of corrugated girders

The zone of post-buckling resistance and its size compared to the pre-buckling zone is a significant factor characterizing the corrugated-web girders. The pre-buckling resistance is the zone of linear displacements from the moment of load application to the moment of buckling load, that is, the moment of the web instability between the load levels 0 – $P_1(P_{eB})$. On the other hand, the zone of post-buckling resistance is the zone of non-linear displacements from the moment of local instability of the web at the point $P_1(P_{eB})$ until the web failure while reaching the buckling load P_{uR}.

The zones of pre- and post-buckling resistance are shown for the exemplary LDP (Load-Displacement Path) $P(y)$ experimental girders M 1.51 with the non-rigid end post and M 2.51 with the stiffened end post (Fig. 16). Coordinates of characteristic points$P_1(P_{eB})$ and $P_2(P_{uR})$ with the corresponding resistance zones are presented in the diagrams.

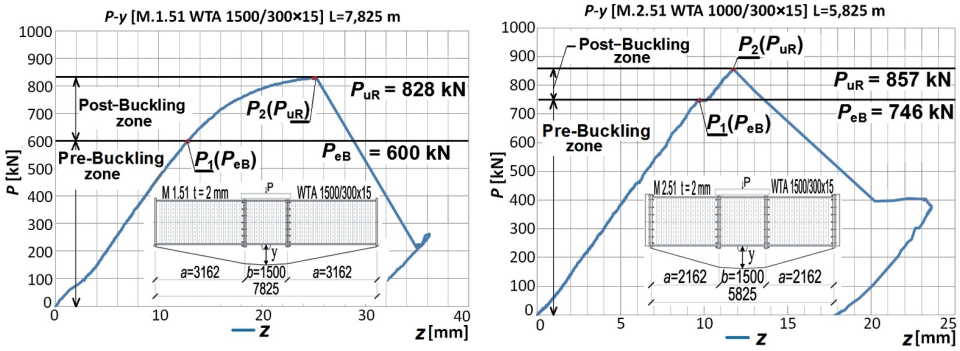

(a) (b)

Fig. 16. LDP's $P(y)$ of experimental beams with a buckling and post-buckling compartment: a) M 1.51 stiffener 25 × 300, b) M 2.51 stiffener 25 × 300 + tee

For the girders with the corrugated web, the efforts should be made to optimize, that is, enlarge the pre-buckling zone 0–$P_1(P_{eB})$, and simultaneously to reduce the post-buckling resistance zone, and to balance the shear resistance against the bending resistance. Such an effect was observed due to stiffness of the support stiffener which reduced the post-buckling zone (Fig. 17b). The impact of stiffness of the support stiffener on the variation of the post-buckling zone in the function of the girder height is illustrated in Fig. 17a and 17b.

For the girders with non-rigid end posts, the widest pre-buckling zone was found for the girders with a web depth h_w = 500 and 1000 mm. With an increasing resistance of the girders, the zone was narrowing with a simultaneous widening of the zone of post-buckling resistance.

Stiffening of the support stiffener in the girders with the stiffener at the free end resulted in widening the pre-buckling zone 0–$P_1(P_{eB})$ whilst the post-buckling zone $P_1(P_{eB})$–$P_2(P_{uR})$ of the girders was reduced. The lowest value for the post-buckling zone was

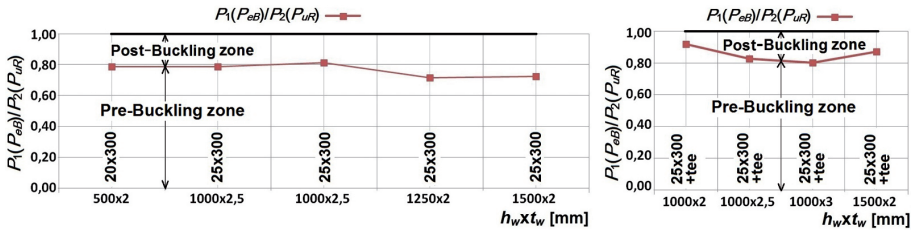

(a)

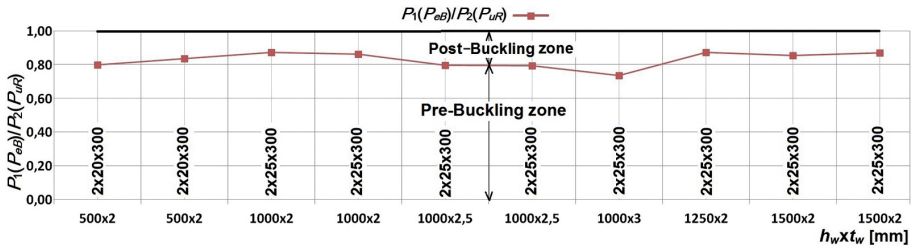

(b)

Fig. 17. Buckling and post-buckling zones of experimental girders with support stiffeners: a) with support stiffeners at the free end, b) with one-sided cantilever

observed for the girder with a web depth $h_w = 1500$ mm. The effect of increasing the pre-buckling zone was slightly reduced with an increasing height of the web, that is, with an increasing ratio between the support stiffener slenderness and the relative slenderness of the web. Behaviour of the girders with a single cantilever was similar to that of the girders with the stiffened end post, which led to an increased pre-buckling zone while the post-buckling zone was reduced.

A change in the range of the pre- and post-buckling zones of the numerical girders in the function of the web depth and thickness related to stiffness of the support stiffeners is shown in Fig. 18a, 18b (with the stiffener at the free end) and in Fig. 18c (with a single cantilever).

For the numerical girders with non-rigid end post, the pre-buckling zone was found to be constant or greater when compared to the experimental girders. Stiffening of the support stiffener with a tee in the girders with the non-rigid end post also resulted in a slightly wider pre-buckling zone 0–$P_1(P_{eB})$ whilst the post-buckling zone $P_1(P_{eB})$–$P_2(P_{uR})$ of the girders was reduced. On the other hand, for the girders with a single cantilever the pre-buckling zone was enlarged with a reduced post-buckling zone.

Taking into account the pre- and post-buckling behaviour of the corrugated web in the SIN girders, stiffness of the support stiffeners was found to increase the pre-buckling zone and reduce the post-buckling one. However, the support stiffener did not stop the induced process of the web failure. For the interactive failure mode, the loss of the stability of

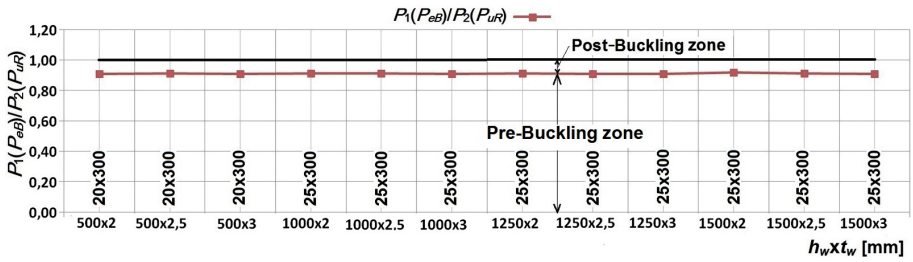

(a)

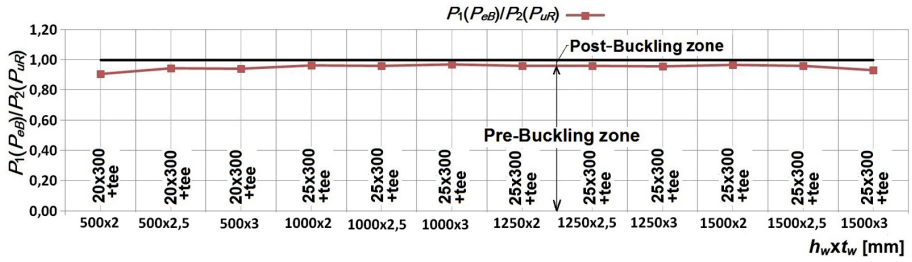

(b)

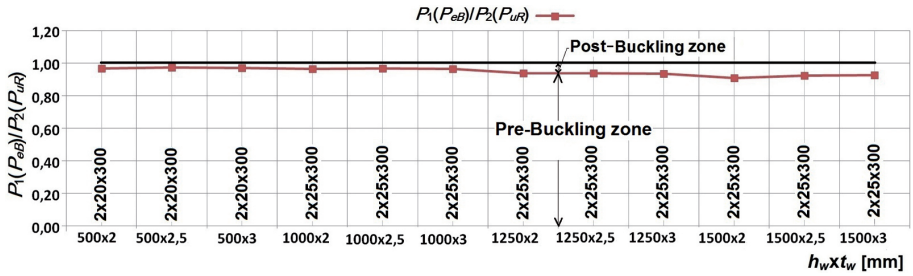

(c)

Fig. 18. Pre-Buckling and post-buckling zones of numerical girders with support stiffeners: a) non-rigid end post, b) stiffened end post, c) with one-sided cantilever

the corrugated web was a very rapid and irreversible process in the final phase. The girder flanges were finally bent, that is, the web frame made of flanges and stiffeners was destroyed.

Thus, the zone of post-buckling resistance was useless to be applied in practice. From the standpoint of the structural reliability, however, the post-buckling zone provided a yield delay, i.e. it may be regarded as a safety margin [17]. Due to irreversibility of the buckling failure process for the corrugated web, the design shear resistance V_{Rd} for the pre-buckling zone should be determined according to equation (1.3–1.6). Hence, the efforts should be made to increase as much as possible the pre-buckling resistance to the level of the resistance limit.

6. Conclusions

The web-corrugated girders with support stiffeners are statically the non-determinable internal structure.

The corrugated webs of girders suffered local, and also mutually interrelated local and global stability failure. The yield lines on the web were immediately formed in the shallow girders with a web depth $h_w = 500$ mm, where the local buckling in the corrugated web was observed near the tension flange. However, in the web depth starting with $h_w = 1000$ mm, local stability failure of the web was initiated simultaneously at several points, starting from the local buckling between the tension flange and the girder axis. Then, the failure evolved to the global mode. The local instability initiated the mechanism of the web failure and led to the global buckling of the web, causing the interaction between both failure modes.

The performed tests showed that increasing stiffness of the support stiffeners in web-corrugated girders had an influence on the size of pre- and post-buckling resistance zones, which consequently reduced the zone of post-buckling resistance.

The post-buckling zone for the web-corrugated girders was the zone for both strains and non-linear displacements of the web. That zone was regarded as not acceptable for use because the initiated loss of stability was an irreversible and rapid process, and the resulting displacements in the non-linear area were permanent. From the standpoint of the structural reliability, however, the post-buckling zone provided a yield delay, i.e. it may be regarded as a safety margin. The experimentally-determined reserves of resistance for the corrugated-web girders ranged from 19% to 21% for the girders with the non-rigid end post, and from 8% to 21% for the girders with the stiffened end post. The results obtained from the numerical analysis were slightly lower and ranged from 8% to 9% for the girders with the non-rigid end post, and from 3% to 9% for the girders with the stiffened end post.

The estimation of the resistance reserves for the web-corrugated girders provided information on possibilities of increasing the pre-buckling resistance by optimizing the structure using, i.e., the stiffened end posts or allowable diagonals of the tension stiffeners as described in the paper [19].

References

[1] Z. Mendera, K. Kuchta, *Profiles of corrugated web of SIN girders. Principles of dimensioning*. Cracow University of Technology, 2002.

[2] J.T. Easley, "Buckling formulas for corrugated metal shear diaphragms", *Journal of the Structural Division*, 1975, vol. 101, no. 7, pp. 1403–1417.

[3] *EN 1993-1-5:2006 Eurocode 3*: *Design of steel structures – Part 1-5: Plated structural elements*. European Committee for Standardization, Brussels, Belgium, 2008. http://www.phd.eng.br/wp-content/uploads/2015/12/en.1993.1.5.2006.pdf.

[4] K. Kuchta, "Nośność i sztywność blachownic o falistych środnikach", Ph.D. thesis, Politechnika Krakowska, Wydział Inżynierii Lądowej Politechniki Krakowskiej, Kraków, 2004.

[5] M. Piekarczyk, *Selected design problems of thin-walled steel members and connections in building structures*. Kraków: Wydawnictwo Politechniki Krakowskiej, 2019.

[6] J. Rutecki, *Cienkościenne konstrukcje nośne*. *Obliczenia wytrzymałościowe*. Warszawa: PWN, 1966.

[7] A. Piekarczuk, P. Więch, K. Kuczyński, R. Walentyński, "Experimental and computational approaches to the evaluation of double corrugated arch structures. A review of the latest advancements", *Archives of Civil Engineering*, 2021, vol. 67, no. 2, pp. 7–35; DOI: 10.24425/ace.2021.137152.

[8] H.H. Abbas, R. Sause, R.G. Driver, "Shear strength and stability of high performance steel corrugated web girders", in *SSRC Conference*. 2002, pp. 361–387.

[9] R.G. Driver, H.H. Abbas, R. Sause, "Shear behavior of corrugated web bridge girders", *Journal of Structural Engineering*, 2006, vol. 132, no. 2, pp. 195–203; DOI: 10.1061/(ASCE)0733-9445(2006)132:2(195).

[10] M. Elgaaly, R.W. Hamilton, A. Seshadri, "Shear strength of beams with corrugated webs", *Journal of Structural Engineering*, 1996, vol. 122, no. 4, pp. 390–398; DOI: 10.1061/(ASCE)0733-9445(1996)122:4(390).

[11] R.W. Hamilton, "Behavior of welded girder with corrugated webs", Ph.D. thesis, University of Maine, USA, 1993.

[12] J. Moon, J. Yi, B.H. Choi, H. Lee, "Shear strength and design of trapezoidally corrugated steel webs", *Journal of Constructional Steel Research*, 2009, vol. 65, pp. 1198–1205; DOI: 10.1016/j.jcsr.2008.07.018.

[13] E.Y. Sayed-Ahmed, "Behavior of steel and (or) composite girders with corrugated steel webs", *Canadian Journal of Civil Engineering*, 2001, vol. 28, no. 4, pp. 656–672; DOI: 10.1139/l01-027.

[14] R. Sause, T.N. Braxtan, "Shear strength of trapezoidal corrugated steel webs", *Journal of Constructional Steel Research*, 2011, vol. 67, no. 2, pp. 223–236; DOI: 10.1016/j.jcsr.2010.08.004.

[15] J. Yi, H. Gil, K. Youm, H. Lee, "Interactive shear buckling behavior of trapezoidally corrugated steel webs", *Engineering Structures*, 2008, vol. 30, pp. 1659–1666; DOI: 10.1016/j.engstruct.2007.11.009.

[16] M.E.A.-H. Eldib, "Shear buckling strength and design of curved corrugated steel webs for bridges", *Journal of Constructional Steel Research*, 2009, vol. 65, no. 12, pp. 2129–2139; DOI: 10.1016/j.jcsr.2009.07.002.

[17] Projekt badawczy N N506 072538, *Kształtowanie konstrukcji szkieletowych z dźwigarów o falistym środniku łączonych doczołowo*. Gliwice: Politechnika Śląska, 2013.

[18] W. Basiński, "Shear buckling of plate girders with corrugated web restrained by end stiffeners", *Periodica Polytechnica Civil Engineering*, 2018, vol. 62, no. 3, pp. 757–771; DOI: 10.3311/PPci.11554.

[19] W. Basiński, *Nośność dźwigarów o falistym środniku wzmocnionych żebrami podporowymi i przekątnymi*. Gliwice: Wydawnictwo Politechniki Śląskiej, 2020.

[20] Abaqus software adjustment to estimate resistance of corrugated web girders reinforced with end stiffeners. This research was supported in part by PL-GRID infrastructure, and also by the WIND grant.

[21] *EN 10002-1:2001 Metallic materials – Tensile testing – Part 1: Method of test at ambient temperature*. European Committee for Standardization, Brussels, Belgium, 2001.

[22] W. Basiński, Z. Kowal, "Random strength parameters of steel corrugated webs and their influence on the resistance of SIN plate girders", *Architecture Civil Engineering, Environment*, 2018, vol. 11, no. 3, pp. 65–77; DOI: 10.21307/ACEE-2018-039.

[23] B.A. Memon, Xz. Su, "Arc-length technique for nonlinear finite element analysis", *Journal of Zhejiang University SCIENCE*, 2004, vol. 5, pp. 618–628; DOI: 10.1631/jzus.2004.0618.

Pokrytyczne zapasy nośności dźwigarów o falistym środniku z żebrami podporowymi

Słowa kluczowe: element skończony, dźwigar o falistym środniku typu SIN, strefa nadkrytyczna, nośność na ścinanie, żebro podporowe

Streszczenie:

Analiza dźwigarów o faliście wyprofilowanym środniku jak i środniku trapezowym koncentruje się na opisie nośności krytycznej, ewentualnie nośności granicznej pomijając przedział nośności nadkrytycznej dźwigarów. Problemem otwartym pozostaje zatem przedział nośności nadkrytycznej

i jego możliwość wykorzystania w praktyce.W tym celu w niniejszej pracy przedstawiono analizę badań nośności postaciowej falistego środnika dźwigarów SIN z żebrami podporowymi w zakresie do i pokrytycznym.

Badania doświadczalne przeprowadzono na dwudziestu dźwigarach o wysokości środnika 500, 1000, 1250 i 1500 mm złożonych z trzech elementów wysyłkowych. Dźwigary o schemacie statycznym belki swobodnie podpartej oraz belki swobodnie podpartej z jednostronnym wspornikiem zbudowano z elementów wysyłkowych połączonych doczołowo na śruby sprężone.

Z kolei analizę numeryczną FEM przeprowadzono na modelach o wysokościach środnika od h_w = 500 do 1500mm przy pełnym zakresie grubości środnika 2,0; 2,5 i 3 mm.

W celu określenia początku niestateczności falistego środnika przeanalizowano przebiegi odkształceń na ukośnych tensometrach naklejonych na środniku. Tensometry naklejono w postaci rozety na kierunku spodziewanych największych odkształceń. Kąt pomiędzy tensometrami w rozetach wynosił 120°. Na podstawie charakteru wykresów odkształceń określono punkt początkowy utraty stateczności falistego środnika, wiążąc z nim obciążenie krytyczne P_{eB}, które przyjęto w punkcie utraty liniowego charakteru zależności obciążenia od odkształcenia $P(\varepsilon)$.

Analizując proces utraty stateczności falistego środnika rozróżniono zniszczenie dźwigarów niskich o h_w = 500 mm i wysokich od h_w = 1000 mm przyporządkowując im punkty utraty stateczności rozgraniczające obszar dokrytyczny oraz nadkrytyczny.

W przypadku dźwigarów niskich o wysokości środnika 500 mm z żebrami podporowymi opisano lokalny proces zniszczenia środnika. Z koeli w przypadku dźwigarów o wysokości środnika od h_w = 1000 mm stwierdzono wzajemne powiązanie lokalnej oraz globalnej postaci zniszczenia prowadzące do ich interakcji.

W wyniku przeprowadzonych badań wykazano, że w dźwigarach o falistym środniku występuje wpływ sztywności żeber podporowych na wielkość przedziałów do i nadkrytycznego, prowadząc do redukcji przedziału nadkrytycznego nośności dźwigarów.

W dźwigarach o falistym środniku przedział nadkrytyczny jest przedziałem zarówno odkształceń jak i przemieszczeń nieliniowych środnika. Stwierdzono, że nie nadaje się jednak do wykorzystania w eksploatacji, gdyż zapoczątkowany proces utraty stateczności jest nieodwracalny oraz gwałtowny, a powstałe przemieszczenia w obszarze nieliniowym są trwałe. Stanowi natomiast z punktu widzenia bezpieczeństwa zabezpieczenie przed katastrofą w postaci przystanku plastycznego. Zapas nośności dźwigarów o falistym środniku wyniósł wg badań doświadczalnych od 19% do 21% w dźwigarach z podporowym żebrem podatnym oraz od 8% do 21% w dźwigarach z podporowym żebrem sztywnym. W przypadku analizy numerycznej był nieco mniejszy i oscylował w przedziale od 8% do 9% w dźwigarach z podporowym żebrem podatnym oraz od 3% do 9% w dźwigarach z żebrem podporowym usztywnionym. Oszacowanie nadwyżki nośności dźwigarów o falistym środniku dało odpowiedź o możliwościach zwiększania nośności dokrytycznej w drodze optymalizacji konstrukcji, np. poprzez zastosowanie usztywnionych żeber podporowych, czy też możliwych przekątnych żeber rozciąganych.

Received: 2022-06-09, Revised: 2022-08-18